Brain Struct Funct (2015) 220:3683–3699
DOI 10.1007/s00429-014-0883-9

ORIGINAL ARTICLE

Evidence for multiple sensory circuits in the brain arising from the respiratory system: an anterograde viral tract tracing study in rodents

Alice E. McGovern · Nicholas Davis-Poynter · Seung-Kwon Yang · David G. Simmons · Michael J. Farrell · Stuart B. Mazzone

Received: 24 February 2014 / Accepted: 20 August 2014 / Published online: 27 August 2014

Abstract Complex sensations accompany the activation of sensory neurons within the respiratory system, yet little is known about the organization of sensory pathways in the brain that mediate these sensations. In the present study, we employ anterograde viral neuroanatomical tract tracing with isogenic self-reporting recombinants of HSV-1 strain H129 to map the higher brain regions in receipt of vagal sensory neurons arising from the trachea versus the lungs, and single-cell PCR to characterize the phenotype of sensory neurons arising from these two divisions of the respiratory tree. The results suggest that the upper and lower airways are predominantly innervated by sensory neurons derived from the somatic jugular and visceral nodose cranial ganglia, respectively. This coincides with central circuitry that is predominately somatic-like, arising from the trachea, and visceral-like, arising from the lungs. Although some convergence of sensory pathways was noted in preautonomic cell groups, this was notably absent in thalamic and cortical regions. These data support the notion that distinct afferent subtypes, via distinct central circuits, subserve sensations arising from the upper versus lower airways. The findings may explain why sensations arising from different levels of the respiratory tree are qualitatively and quantitatively unique.

Keywords HSV-1 H129 · Isogenic recombinant viruses · Transynaptic · Somatosensory · Viscerosensory · Airway sensations

A. E. McGovern (✉) · S.-K. Yang · D. G. Simmons · S. B. Mazzone
School of Biomedical Sciences, The University of Queensland, St Lucia, QLD 4072, Australia
e-mail: a.mcgovern1@uq.edu.au

S. B. Mazzone
e-mail: s.mazzone@uq.edu.au

N. Davis-Poynter
Clinical Medical Virology Centre/Queensland Children's Medical Research Centre, The University of Queensland and Sir Albert Sakzewski Virus Research Centre, Royal Children's Hospital, Brisbane, QLD 4029, Australia

M. J. Farrell
Department of Medical Imaging and Radiation Sciences, Monash University, Clayton, VIC 3800, Australia

Introduction

The respiratory system is densely innervated by vagal sensory nerve fibers, the activation of which is known to contribute substantially to the symptoms of pulmonary disease. These symptoms notably include cough, mucous secretion, bronchospasm and airway wall edema, all of which occur via well-described reflex pathways that regulate brainstem autonomic and respiratory motor outputs (Shannon et al. 2004; Haxhiu et al. 2005; Mazzone et al. 2005; McGovern and Mazzone 2010; Mazzone and Canning 2013). However, the activation of pulmonary sensory nerves can also induce complex respiratory sensations including dyspnea and the perception of airways irritation leading to the urge to cough. These sensations are contingent on ascending sensory inputs to higher brain regions that encode perceptual awareness of the pulmonary environment (Mazzone et al. 2007; Davenport and Vovk 2009; Evans 2010; Mazzone et al. 2011). However, unlike reflexive neural pathways, our understanding of higher brain sensory pathways arising from the respiratory system is limited.

A growing body of evidence indicates that the primary sensory neurons innervating the airways are not homogenous. Indeed, subtypes can be delineated based on

functionality, anatomy and neurochemistry, but perhaps more interestingly they can also be differentiated based on embryological origin (Kummer et al. 1992; Riccio et al. 1996; Undem et al. 2004; Mazzone and McGovern 2008; Nassenstein et al. 2010). For example, in mice and guinea pigs, vagal sensory neurons innervating the upper airways (larynx/trachea) are principally derived from the jugular cranial ganglia and somatic tissues of the neural crest of embryological origin (comparable to the dorsal root ganglia of the spinal cord). This is in contrast to the sensory innervation of the lower airways (lungs) which displays characteristics of being derived from the nodose cranial ganglia derived from the epibranchial placodes that form the visceral nervous system (Undem et al. 2004; Kwong et al. 2008; Nassenstein et al. 2010; Lieu et al. 2011). This embryological distinction raises important questions about the central organization of sensory pathways arising from the upper versus lower airways, which might in turn provide insights into the perceptual processing of respiratory sensations.

Previously, we have reported the development of a novel method for mapping intact sensory neural circuits in animal models using a genetically modified herpes simplex virus 1 (HSV-1), strain H129 (McGovern et al. 2012b). HSV-1 H129 is unique inasmuch as it infects neurons, moves along axons and can pass between synaptically connected neurons preferentially, albeit not exclusively, in the anterograde direction (Garner and LaVail 1999; Rinaman and Schwartz 2004; Song et al. 2008; Lo and Anderson 2011; McGovern et al. 2012a, b; Vaughan and Bartness 2012; Wojaczynski et al. 2014). Thus, insights into the organization of complex neural circuits can be made by following the successive pattern of HSV-1 H129 infection throughout the nervous system subsequent to central or peripheral inoculation. Using this tool we have shown that at least two ascending neural pathways arise from the upper airways (extrathoracic trachea), one which follows the trigeminothalamocortical tracts (from the brainstem to ventrobasal thalamus and onto the sensory cortex) and a second via a thalamolimbic circuit (from the brainstem to the mediodorsal and/or submedius thalamus to the rostral agranular insular/lateral orbital and cingulate cortices) (McGovern et al. 2012a, b). This circuitry is somewhat analogous to the lateral and medial pain pathways described for processing of noxious stimuli arising from somatic tissues (Jasmin et al. 2004; Tang et al. 2009; Whitt et al. 2013). Notably, HSV-1 H129 following tracheal inoculation does not appear in the 'visceral thalamus' (ventrobasal parvicellular thalamus), a region of the thalamus shown to be in receipt of afferent pathways from other viscera (Allen et al. 1991). These observations might suggest that upper airway sensory pathways ascend into the brain via circuits that resemble those described for somatic noxious sensory processing. In the present study, we set out to compare the organization of upper airway sensory circuitry in the brain to that arising from the lower airways, to assess the possibility that distinct neural circuits underpin sensory processing arising from differentially innervated regions of the respiratory system.

Methods

All experiments were approved by the University of Queensland Institutional Animal Ethics Committee. Experiments were performed on adult male Sprague–Dawley rats (150–250 g), which were individually housed in a standard environment and given ad libitum access to water and food. All efforts were made to minimize the number of animals used and their suffering.

Conventional retrograde tracing of vagal sensory neurons innervating the trachea and lung

Rats ($n = 6$) were anesthetized with 5 % isoflurane in an induction chamber and maintained at 2.5 % in medical oxygen via a nose cone. 5 µl of 0.5 % DiI (2 % stock in DMSO, diluted to a final concentration in sterile saline) was administered to either the trachea or lung. For tracheal injections, the extrathoracic trachea was exposed via a ventral midline incision in the animal's neck as previously described (Mazzone and McGovern 2006, 2008; McGovern and Mazzone 2010; McGovern et al. 2012a, b) and the dye was injected into the lumen of the trachea two cartilage rings caudal to the larynx. For lung injections, the left lung was injected from the posterior side of the animal and through the seventh intercostal space as previously described by others (Undem et al. 2004). Briefly, skin and external intercostal musculature was retracted, the lung visualized underneath the intact internal intercostals and, using a 30G needle attached to a 10 µl gastight Hamilton syringe, 5 µl of DiI was injected into the left lung lobe. The needle was left in place for 60 s to limit the spread of dye onto surrounding tissues. The incisions were sutured and animals were allowed to recover for up to 2 weeks. An analgesic, meloxicam (1 mg/kg, s.c.), was administered prior to the end of each surgery.

Single-cell isolation

To identify vagal sensory neurons traced from either the trachea or lung, animals were euthanized with an overdose of sodium pentobarbital (100 mg/kg i.p) and their vagal ganglia dissociated as previously described (Kalous and Keast 2010). Briefly, ganglia were removed and freed from surrounding connective tissue and placed into a tube

containing an enzymatic solution of collagenase (Type I) and trypsin/EDTA dissolved in modified Tyrodes solution (Kalous and Keast 2010) and bubbled with 95 % oxygen and 5 % carbon dioxide. The cells were gently triturated with fire-polished glass Pasteur pipettes of decreasing diameter, washed with modified Tyrodes and centrifuged at 500*g* to remove myelin and cellular debris. Cells were then resuspended in Neurobasal A medium containing B27 supplement, Glutamax I and antibiotic/mycotic solution (Life technologies) and plated out onto the center of poly-L-lysine coated coverslips and incubated at 37 °C with 5 % carbon dioxide. Two hours after plating, the cells were washed twice with complete Neurobasal A medium and flooded with fresh medium. Within 4 h of dissociation, cells were identified by fluorescence microscopy and single traced neurons were collected by suction with RNase-free glass pipettes (tip diameter 20–70 µm) pulled with a micropipette puller (P-97 Micropipette Puller, Sutter Instrument Company). The pipette tips were broken into a PCR tube containing resuspension buffer and RNase OUT (Life technologies), snap frozen and stored at −80 °C. Samples of cell culture medium adjacent to cells were collected as negative controls.

Single-cell RT-PCR

Cells were processed using the SuperScript III CellsDirect cDNA synthesis kit (Life Technologies) according to the manufacturer's instructions and following previously described methods (Lieu et al. 2011). A total of 27 cells traced from the trachea and 23 cells traced from the lung were successfully collected and processed for RT-PCR, to characterize each cell as either of placodal (nodose) or neural crest (jugular) origin based on their differential expression of TRKA, TRKB, PPT-A and P2X2 (Undem et al. 2004; Kwong et al. 2008; Nassenstein et al. 2010; Lieu et al. 2011). TRPV1 expression was also assessed for delineating C-fiber afferents. For RT-PCR we utilized a nested primer approach. The first PCR reaction contained 1 unit of Hot Start My Taq Polymerase (Bioline), with PCR buffer, primers (Table 1, outer primer pair) for beta-actin, TRPV1, TRKA, TRKB, PPT-A and P2X2 and template (1.5 µl cDNA, no RT control or bath control). Whole rat vagal ganglion tissue was run as a positive control. The PCR conditions included 40 cycles with an initial denaturation at 98 °C for 1 min, denaturation at 98 °C for 10 s, annealing at 58 °C for 15 s and extension at 72 °C for 15 s, followed by a final extension at 72 °C for 10 min. The second PCR reaction contained 1 unit of Hot Start My Taq Polymerase (Bioline), with PCR buffer, primers internal to the first primer binding sites (Table 1, inner primer pair) for beta-actin TRPV1, TRKA, TRKB, PPT-A and P2X2 and template (1 µl of product from first reaction). Negative control samples (culture media) were processed in parallel. Products were visualized by electrophoresis on ethidium bromide-stained 2 % agarose gels.

Construction of self-reporting HSV1-H129 viral tracers

We have previously reported in detail the construction of the anterograde viral tracer HSV-1 H129 EGFP (McGovern et al. 2012b), and following the same protocol we generated and characterized an isogenic viral recombinant expressing tdTomato. As part of this characterization, we performed intra-tracheal injections of the tdTomato virus (see below) to compare the central pattern of infection obtained with this recombinant to that which we have previously reported (McGovern et al. 2012a, b). All viral stocks were propagated on Vero cells and then concentrated by ultracentrifugation (106,000*g* for 3 h 30 min at 4 °C, with the pellet resuspended in sterile PBS) to a final titer of 1×10^9 pfu/ml. Aliquots were stored frozen at −80 °C until the time of in vivo inoculation. Procedures involving live HSV-1 H129 virus were conducted in accordance with Biosafety level 2 standards.

Viral inoculations

Using the same surgical techniques as described above for DiI injections, animals were inoculated with 10 µl of 1×10^9 pfu/ml of either HSV-1 tdTomato or 5 µl HSV-1 H129 EGFP into the tracheal lumen ($n = 18$) or left lung ($n = 16$), respectively. After inoculation, the wound was sutured and animals were allowed to recover for 48–96 h (denoted 'early time point', $n = 9$), 96–120 h (denoted as 'mid time point', $n = 11$) and 120–168 h (denoted 'late time point', $n = 14$). In separate experiments to assess the levels of divergence and/or convergence in the brain of sensory inputs arising from the trachea and lung, dual inoculation of both tdTomato (into trachea) and EGFP (into lung) viruses was performed simultaneously ($n = 7$) and animals were killed at 96–168 h p.i.

Tissue harvest

After the designated survival time, animals were overdosed with sodium pentobarbital (100 mg/kg i.p.) and transcardially perfused with 300 ml of 5 % sucrose in 0.1 M phosphate buffered saline (PBS, pH 7.4) followed by 300 ml of 4 % paraformaldehyde (in PBS, pH 7.4). Left and right vagal ganglia, brain and trachea/lung were collected from all animals. Tissues were post-fixed in 4 % paraformaldehyde overnight at 4 °C and then cryoprotected in 20 % sucrose at 4 °C. Tracheae were opened longitudinally along the ventral surface and pinned flat in a Sylgard-filled viewing chamber such that the mucosal

Table 1 Primer sequences for single-cell RT-PCR

Gene	Primer	Sequence	Product length (bp)[a]
β-Actin	Forward outer (5′–3′)	GTGGGCCGCTCTAGGCACCAA	420
	Reverse outer (5′–3′)	CTCTTTGATGTCACGCACGATTTC	
	Forward inner (5′–3′)	GACTCCTATGTGGGTGACGAGG	
	Reverse inner (5′–3′)	GGATCTTCATGAGGTAGTCCGTCA	
TRPV1	Forward outer (5′–3′)	CTTACAGCAGCAGTGAGACC	239
	Reverse outer (5′–3′)	CCATGGAAGCCACATACTCC	
	Forward inner (5′–3′)	AGTTCTCTTTCCCCTACTGA	
	Reverse inner (5′–3′)	AGCAAGAAAGACCTTTCCAA	
TRKA	Forward outer (5′–3′)	CAAATTTGGGATCAACCGCC	162
	Reverse outer (5′–3′)	GCAGACTCCAAAGAAGCGTA	
	Forward inner (5′–3′)	AGTTCTCTTTCCCCTACTGA	
	Reverse inner (5′–3′)	AGCAAGAAAGACCTTTCCAA	
TRKB	Forward outer (5′–3′)	AGCTGGATAACCCCACTCAT	214
	Reverse outer (5′–3′)	AAGAAGACGGAGTGTTGCTC	
	Forward inner (5′–3′)	AACTGACATCGGGGATACTA	
	Reverse inner (5′–3′)	ATCGTCGTTGCTGATGAC	
PPT-A	Forward outer (5′–3′)	AAACGGGATGCTGATTCCTC	221
	Reverse outer (5′–3′)	TGTCTTTGGAGACTGCATCG	
	Forward inner (5′–3′)	AAACAAGTGGCCCTGTTAAA	
	Reverse inner (5′–3′)	TTATTTTACCGCTCACTGCT	
P2X2	Forward outer (5′–3′)	TTCAGGAGAGGGACATCCAG	153
	Reverse outer (5′–3′)	GTCTGAATGGCAGGTAGAGC	
	Forward inner (5′–3′)	GAATACGTAAAGCCCCCG	
	Reverse inner (5′–3′)	CTCGATCCTGGTGATGATG	

[a] Product length refers to inner product only

surface could be viewed as a whole mount preparation for assessment of tdTomato-expressing cells. Vagal ganglia, lung and brains were frozen in OCT-embedding compound, and brain sections (50 μm), ganglia and lung sections (30 μm) were cut using a Hyrax C60 cryostat. Brain sections, from the olfactory bulbs to the spinomedullary junction, were collected in series into 0.1 M PBS. Every second section (i.e., at 100 μm intervals) was mounted onto gelatin-coated slides and screened for tdTomato and/or EGFP fluorescence (infected neurons). When infected neurons were observed, the corresponding adjacent section was subsequently immunostained (free floating) using mouse anti-parvalbumin or rabbit anti-calbindin antisera (1:500; Swant, Bellinzona, Switzerland) to provide morphological detail for delineating the loci of infected neurons. Vagal ganglia and lung sections were thaw mounted onto gelatin-coated slides immediately after sectioning and coverslipped and viewed for tdTomato and/or EGFP fluorescence.

Data analysis

All tissues were examined for HSV-1 immunoreactivity using an Olympus BX51 microscope and representative images were captured with an Olympus DP72 camera. Brain regions were delineated and named according to the nomenclature defined in the Chemoarchitectonic Atlas of the Rat Brainstem and Forebrain (Paxinos et al. 1999a, b) with the exception of the rostral agranular insular cortex (RAIC) which was defined as the agranular insular/lateral orbital cortices from 1.70 to 3.70 mm rostral to the bregma (Burkey et al. 1999; Jasmin et al. 2003, 2004). Representative digital images were imported into Adobe Photoshop CS4 (version 11.0) and optimized (minimally) for brightness, contrast and size for preparation of representative photomicrographs.

Infected vagal ganglia cells arising from either the trachea or lung were quantified separately in the left and right vagal ganglia at 72–96 h p.i. (time of peak infection) as previously described (McGovern et al. 2012a, b). For the brain, every second section collected was first qualitatively assessed for absence or presence of infected neurons and this was used to calculate the proportion of animals in which virus was present in any given region of interest. Subsequently, quantitative cell counts of the number of infected cells in each brain region were performed at 200 μm intervals to limit the possibility of recounting the

same cells in adjacent sections. Hemispheric laterality of infection was assessed for lung only, as it was not possible to meaningfully distinguish hemispheric differences arising from the trachea given its midline position. All cell counts represent the mean ± the standard error of the mean (SEM) of the total number of infected cells per ganglia or brain region at the p.i. times indicated. Student's t tests were performed to assess differences between the numbers of infected neurons where appropriate. In all instances $p \leq 0.05$ was considered to be significant. Pearson's correlation analyses were used to investigate the relationship between the number of infected vagal ganglia neurons and the number of infected neurons in the brainstem nuclei of interest. The ratio of neurons infected in brain regions of interest following tracheal or lung inoculations was assessed by calculating the sum total of all infected neurons and expressing the trachea versus lung infected regions as a percentage of the sum total.

Results

Molecular characterization of vagal sensory neurons innervating the trachea and lungs

Consistent with previous studies conducted on guinea pigs and mice, two broad phenotypes of airway vagal sensory neurons collected from the vagal ganglia of rats could be identified based on the expression of TRKA versus TRKB and PPTA versus P2X2. Thus, tracheal vagal afferent neurons characteristically expressed TRPV1 (96 % of cells), PPT-A (85 % of cells) and TRKA (67 % of cells), whereas fewer expressed TRKB (33 % of cells) or the P2X2 receptor (11 % of cells) (Fig. 1). By contrast, lung vagal afferent neurons typically expressed: TRPV1 (78 % of cells), TRKB (74 % of cells) or P2X2 (61 % of cells), whereas fewer cells expressed PPT-A (48 % of cells) and TRKA (43 % of cells) (Fig. 1). Of the TRPV1 nociceptor population innervating the trachea, 70 and 85 % expressed TRKA and PPT-A, respectively, compared to the expression of TRKB and P2X2, which were confined to 15 and 11 % of the neurons, respectively. By contrast, in TRPV1-positive lung nociceptors, 44 and 55 % expressed TRKA and PPT-A, respectively, and 72 and 61 % expressed TRKB and P2X2, respectively. Although some neurons showed a complex molecular phenotype, most (>80 %) were delineated by either TRKA/PPT-A or TRKB/P2X2 expression. These data are consistent with the trachea being innervated predominately by jugular ganglia neurons, whereas a mixed population of nodose and jugular ganglia neurons innervates the lungs.

HSV-1 H129 infection of primary sensory and medullary neurons following tracheal and lung inoculations

As previously reported (McGovern et al. 2012a), inoculation of the trachea with HSV-1 H129 resulted in viral

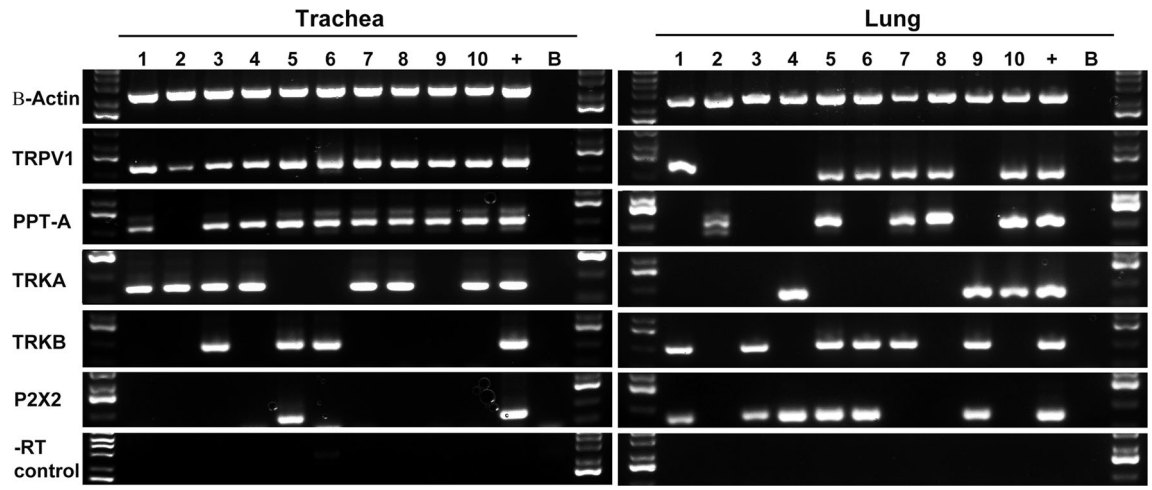

Fig. 1 Characterization of vagal sensory neurons retrogradely labeled from the trachea or lung. The images show single-cell RT-PCR bands of ten representative neurons, each traced from the trachea or lung with DiI and collected from acutely dissociated ganglia. Isolated mRNA from each cell was used both to reverse transcribe (RT) cDNA for assessing gene expression and as a no (−) RT control. Positive (+) control samples of whole vagal ganglia and blank (B) control samples consisting of small volumes of the culture media adjacent to cells were run in parallel. Only cells expressing β-actin were included in the analysis. The majority of traced neurons were nociceptors (defined as expressing TRPV1). Neurons traced from the trachea characteristically expressed PPT-A (i.e., substance P) and the neutrophin receptor TRKA. By contrast, lung sensory neurons characteristically expressed TRKB and the ATP receptor P2X2. See text for percentage expression data

infection (tdTomato expression) in scattered tracheal epithelial cells within a restricted area encompassing three to four cartilage rings (approximately, 6 mm in length) localized to the injection site (2 cartilage rings caudal to the larynx). No viral infection was ever seen in the caudal trachea or indeed in the intrapulmonary airways or lung. By contrast, HSV-1 H129 injection into the lung produced diffuse labelling (EGFP expression) of cells over a wider area (7.4–9.8 mm), but almost exclusively contained within the lung parenchymal tissue or (on occasion) to the walls of small conducting airways. We never saw viral infection in the large airways (bronchi), the trachea or the contralateral lung. Within 48–72 h of inoculating the tracheal lumen with HSV-1 H129 tdTomato, sensory neurons within both the left and right vagal ganglia were robustly infected (Fig. 2a) with no evidence of lateral dominance. Unilateral (left) lung inoculation with HSV-1 H129 EGFP also resulted in infection of sensory neurons in the vagal ganglia. However, unlike tracheal sensory neurons, which were evenly distributed between both the left and right ganglia, cells infected from the left lung were largely and significantly ($p \leq 0.05$) confined ipsilaterally to the left vagal ganglion (Fig. 2a). In total, fewer sensory neurons were infected in the vagal ganglia following viral inoculation of the lung compared to the trachea, possibly reflecting the unilateral nature of the infection, the smaller volume of inoculum (5 versus 10 µl), the differences in tissue architecture between the two injection sites and/or the reported proximal to distal

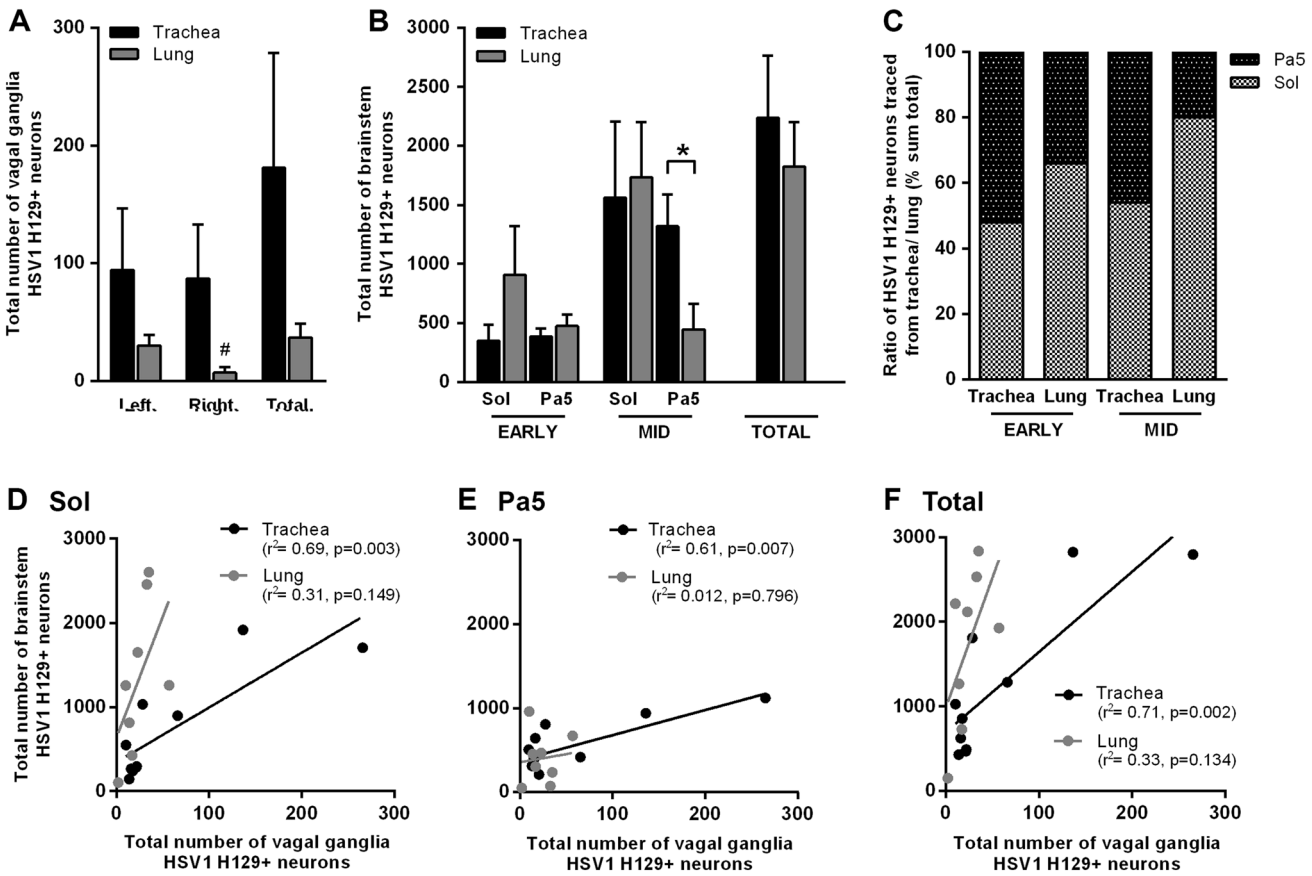

Fig. 2 The relationship between the number of primary sensory and brainstem neurons infected by HSV-1 H129 recombinant viruses following tracheal or lung inoculation. **a** Inoculation of the trachea with HSV-1 H129 resulted in the infection of vagal ganglia neurons, evenly distributed between the left and right ganglia (analyzed at early- and mid-infection time points). By contrast, unilateral lung injection infected fewer neurons and these were significantly confined to the ipsilateral ganglion ($p = 0.05$). **b** Quantification of the number of infected cells in the left nucleus of the solitary tract (Sol) and paratrigeminal nucleus (Pa5) at early- and mid-infection time points. As can be seen, the total number of infected neurons (Sol + Pa5) is not different between tracheal and lung inoculations, despite the fewer vagal ganglia neurons infected. Furthermore, differences are evident in the distribution of tracheal and lung afferent inputs to the Sol and Pa5 (summarized in **c**). **d**, **e** Relationships between the number of vagal ganglia neurons infected (from the trachea or lung) and the resultant number of neurons infected in the Sol, Pa5 or both (total). Of note is the steepness of the lung regression line in **d**, indicative of lung afferents synapsing with many more Sol neurons than do tracheal afferents. Data (**a**, **b**) represent the mean ± SEM of infected cell soma counted from $n = 9$ animals. $^{\#}$Significant difference ($p < 0.05$) when comparing infected neurons in the left and right vagal ganglia following lung inoculation. $^{*}p < 0.05$. See text for additional details

reduction in nerve fiber density that occurs along the tracheobronchial tree (Larson et al. 2003).

Evidence for viral infection within the central nervous system was not seen until 72 h p.i., (for both the trachea and lung inoculations), and at the early time points surveyed (72–96 h p.i.), the virus was limited to the brainstem nuclei (bilaterally for tracheal injections and predominately ipsilaterally for lung injections; Table 2). This notably began with the appearance of virus simultaneously within caudal regions of the nucleus of the solitary tract (particularly in and around the dorsolateral subnucleus) and a caudal dorsal region of the spinal trigeminal tract and nucleus, in a region that includes the paratrigeminal nucleus (Figs. 2, 3, 4). The distribution of HSV-1 H129 infection in the brainstem following tracheal or lung inoculation was more extensive at mid-infection time points (96–120 h p.i.). This period was characterized by an expansion of the infection in the medullary solitary and trigeminal nuclei, as well as the appearance of the virus in more rostral brainstem regions (see below). Intriguingly, despite the fewer total vagal ganglia neurons that were infected following lung inoculations, there was no difference in the combined *total* number of neurons (i.e., the sum of those in the nucleus of the solitary tract and the paratrigeminal nucleus) subsequently infected in brainstem sensory relay nuclei following lung and tracheal inoculations (Fig. 2b). However, the pattern of medullary infection following tracheal and lung inoculations was not identical. In particular, significantly ($p \leq 0.05$) more paratrigeminal neurons were infected at mid and late time points following tracheal inoculation compared to lung inoculation (Fig. 2b; Table 2). Furthermore, when the total number of infected neurons in the brainstem was considered, differences between the ratios of lung versus tracheal afferent innervated populations became apparent, with lung inoculations appearing to infect neurons preferentially in the nucleus of the solitary tract (Fig. 2c). Indeed, although we noted correlations between the number of infected vagal ganglia neurons and the corresponding number of infected brainstem neurons within individual animals (Fig. 2d, e, f), many more neurons in the brainstem (particularly, in the nucleus of the solitary tract) were infected for each afferent infected from the lung compared to the trachea. This is reflected in the steep slope of the lung regression line (Fig. 2d, f) and suggests a substantial difference in the number of nucleus of the solitary tract neurons in synaptic connectivity with any given lung versus tracheal afferent neuron.

HSV-1 H129 infection of the supramedullary regions following tracheal and lung inoculations

Inoculation of the tracheal lumen or lung with HSV-1 H129 resulted in a time-dependent appearance of fluorescent reporter expression (viral infection) throughout the supramedullary neuraxis (Figs. 3, 4; Table 2). At mid-infection time points (96–120 h p.i.), HSV-1 H129 infection appeared at more rostral brainstem regions (i.e., in pontine and midbrain nuclei) including the parabrachial nuclei (typically, the lateral subnucleus), the Kölliker-Fuse nucleus, locus coeruleus and the periaqueductal gray. The distribution of HSV-1 H129 infection in pontine and midbrain nuclei was bilateral following tracheal inoculation, but predominately ipsilateral to the inoculation site following lung inoculations. Significantly ($p \leq 0.05$) more neurons were infected in the locus coeruleus (at late time points) following tracheal inoculation with virus, whereas we typically noted more cells infected in the periaqueductal gray and parabrachial nuclei following tracheal and lung injections, respectively (Table 2).

Mid- to late-infection time points were characterized by viral infection in a number of subcortical forebrain nuclei. In the thalamus, robust infection was confined to the ventrobasal thalamus (ventral posterolateral and ventral posteromedial nuclei), reticular nucleus, submedius nucleus and mediodorsal nucleus following tracheal inoculations (Fig. 3; Table 2), although a number of other thalamic nuclei contained infected cells (Table 2). In the hypothalamus and subthalamic regions of the same animals, infection was largely confined to the lateral and paraventricular nuclei and the zona incerta (Fig. 3; Table 2). Following lung inoculations, while the contralateral ventrobasal thalamus (particularly the ventral posteromedial nucleus) was routinely infected, the incidence of infection in the reticular, mediodorsal and submedius thalamus was much lower than that observed following tracheal injections (Table 2). Thus, only one animal with a lung injection of virus displayed infection in the mediodorsal thalamus at any time points surveyed, and only two animals had contralateral infections in the reticular and submedius thalamus at late-infection time points. This resulted in significantly fewer total number of infected cells identified in these regions following lung inoculations (Table 2). Significantly fewer infected cells were also noted in the ventral posterolateral thalamus following lung injection of virus. A robust infection was seen within the contralateral parvicellular portion of the ventrobasal complex following lung inoculation, beginning at mid-infection time points (Fig. 4; Table 2). Infection was never seen in this region following tracheal viral inoculation. The location of subthalamic and other subcortical infections was largely comparable between lung and tracheal inoculated animals, although the number of infected cells in regions such as the zona incerta, lateral hypothalamus and paraventricular nucleus in lung-inoculated animals was typically less than in animals injected with virus into the trachea (Table 2).

Table 2 Quantitative analysis of the number of HSV-1 H129 cells located in the brain following inoculation of either the extrathoracic trachea (upper airways) or the left lung (lower airways)

	Early		Mid		Late	
	Trachea ($n = 5$)	Lung ($n = 4$)	Trachea ($n = 6$)	Lung ($n = 5$)	Trachea ($n = 7$)	Lung ($n = 7$)[a]
Hindbrain						
Nucleus of the solitary tract (Sol)	349.9 ± 134.6 (5)	908.5 ± 409.8 (4)[i]	1,560.8 ± 642.8 (6)	1,731.6 ± 470.2 (5)	597.6 ± 84.7 (7)	1,549.9 ± 543.3 (5)
Spinal trigeminal (Sp5)	25.4 ± 17.1 (5)	102.3 ± 58.9 (3)[i]	923.2 ± 257.9 (6)	757.4 ± 230.3 (4)[i]	848.0 ± 210.8 (7)	702.8 ± 166.6 (5)
Spinal trigeminal tract (sp5)	94.8 ± 37.5 (5)	121.5 ± 12.5 (3)[i]	904.0 ± 210.43 (6)	525.6 ± 100.5 (4)[i]	648.9 ± 109.8 (7)	747.2 ± 210.8 (4)
Paratrigeminal (Pa5)	383.9 ± 69.8 (5)	475.0 ± 97.8 (4)[i]	1,318.8 ± 270.9* (6)	443.8 ± 217.66 (3)[i]	573.1 ± 78.0* (7)	295.4 ± 85.5 (4)
Lateral parabrachial (LPB)		22.5 ± 13.4 (2)[i]	68.0 ± 31.7 (4)	150.4 ± 44.3 (4)[i]	155.1 ± 46.3 (6)	181.8 ± 45.3 (5)
Medial parabrachial (MPB)			7.8 ± 5.0 (2)	35.0 ± 21.7 (2)[i]	49.7 ± 22.1 (3)	46.6 ± 21.3 (5)
Kölliker-Fuse (KF)			18.3 ± 18.3 (1)	35.6 ± 21.6 (3)[i]	46.1 ± 15.0 (3)	51.4 ± 23.6 (2)[i]
Locus coeruleus (LC)			121.0 ± 56.0 (3)	55.8 ± 34.0 (3)	320.6 ± 68.6* (7)	75.4 ± 34.2 (3)
Periaqueductal gray (PAG)			55.8 ± 44.3 (2)	29.6 ± 15.3 (2)[i]	376.4 ± 192.8 (7)	84.2 ± 29.5 (5)
Forebrain–diencephalon						
Thalamus						
Mediodorsal thalamus (MD)			14.0 ± 9.38 (2)	–	102.0 ± 43.2* (5)	7.0 ± 7.0 (1)[c]
Posterior thalamic group (Po)			145.6 ± 53.5 (6)	82.8 ± 41.1 (3)[c]	461.0 ± 94.0 (7)	454.8 ± 99.1 (5)[c]
Reticular thalamus (Rt)			95.3 ± 44.1 (3)	–	491.1 ± 134.8* (7)	61.6 ± 36.7 (2)[c]
Submedius thalamus (Sub)			99.0 ± 49.7 (4)	26.8 ± 26.8 (1)[c]	657.6 ± 209.3* (7)	47.1 ± 35.6 (2)[c]
Parafascicular thalamus (PF)			3.3 ± 3.3 (1)	12.0 ± 9.7 (1)	28.4 ± 18.4 (2)	8.5 ± 7.9 (2)[c]
Ventral						
Lateral thalamus (VL)			20.0 ± 20.0 (1)	–	100.0 ± 66.1 (2)	66.4 ± 66.4 (1)[i]
Medial thalamus (VM)			29.2 ± 13.4 (2)	8.4 ± 5.2 (1)[c]	231.4 ± 67.9 (4)	184.7 ± 65.4 (4)
Posterior thalamus, parvicellular part (VPPC)			–	77.0 ± 25.9* (4)[c]	–	121.9 ± 39.5* (4)[c]
Posterolateral thalamus (VPL)			307.2 ± 91.1 (6)	239.6 ± 112.7 (4)[c]	2,223.1 ± 311.8* (7)	707.1 ± 201.6 (5)
Posteromedial thalamus (VPM)			154.2 ± 66.7 (4)	193.4 ± 138.3 (4)[c]	988.1 ± 197.7 (7)	593.9 ± 137.6 (4)
Hypothalamus/other						
Lateral hypothalamic area (LH)			41.3 ± 15.4 (4)	28.6 ± 12.7 (3)	134.6 ± 43.5 (7)	50.9 ± 12.3 (3)
Paraventricular hypothalamus (PaMP, PaV)			39.3 ± 22.1 (3)	26.4 ± 16.9 (1)	212.7 ± 68.1* (7)	40.9 ± 9.3 (4)
Zona incerta (ZI)			228.1 ± 57.9 (6)	137.4 ± 62.0 (2)[c]	767.0 ± 237.4 (7)	469.7 ± 133.8 (5)
Medial lemniscus (ml)			76.9 ± 22.0 (6)	58.0 ± 20.6 (4)[c]	418.6 ± 61.8* (7)	177.0 ± 44.3 (5)
Other subcortical						
Central amygdala (CeA)			13.2 ± 13.2 (1)	57.4 ± 41.2 (2)[i]	104.4 ± 45.7 (5)	84.4 ± 50.6 (4)[i]
Caudate putamen (CPu)					757.4 ± 387.8 (5)	389.7 ± 190.7 (3)
Globus pallidus (GP)					364.3 ± 58.6 (5)	60.7 ± 19.1 (3)
Cortical						
Rostral agranular insular cortex (RAIC)					189.0 ± 87.6 (5)	36.3 ± 32.5 (2)[c]
Agranular insular (AI)					–	21.8 ± 16.8 (2)[c]

Table 2 continued

	Early		Mid		Late	
	Trachea ($n = 5$)	Lung ($n = 4$)	Trachea ($n = 6$)	Lung ($n = 5$)	Trachea ($n = 7$)	Lung ($n = 7$)[a]
Dysgranular insular (DI)					28.8 ± 28.8 (1)	72.6 ± 34.9 (2)[c]
Granular insular (GI)					27.0 ± 23.1 (2)	87.7 ± 45.7 (3)[c]
Cingulate (Cg)					9.71 ± 9.71 (1)	12.8 ± 6.7 (3)[c]
Primary somatosensory (S1)					959.3 ± 549.4 (7)	821.3 ± 407.5 (6)[c]
Secondary somatosensory (S2)					412.86 ± 203.0 (5)	114.9 ± 50.4 (5)[c]
Primary motor (M1)					92.4 ± 62.7 (2)	14.3 ± 7.8 (3)[c]
Secondary motor (M2)					109.7 ± 102.4 (2)	67.6 ± 41.1 (3)[c]

Early, mid and late refer to the time points surveyed after viral inoculation. Data represent the mean ± SEM total number of cells counted for each region listed. Dashes denote 0 ± 0 infected cells. Values in brackets represent the number of animals in the group in which a region was infected

i ipsilateral to the injection site, *c* contralateral to the injection site

* Significant difference between trachea and lung infected brain regions, $p \leq 0.05$

[a] Two lung LATE time point animals in which the subcortical infection had resolved, and only data from the cortical regions were able to be collected

On late infection (120–168 h p.i.), HSV-1 H129 was routinely present in the central subnucleus of the amygdala, globus pallidus and caudate putamen, as well as in cortical brain regions following both tracheal and lung injections. The latter included infection in the rostral agranular insular/lateral orbital cortex (RAIC), more caudal regions of the agranular, dysgranular and granular insular cortex and in layer 4 of the primary and secondary somatosensory cortices (Figs. 3, 4; Table 2). We consistently saw more infected cells in the RAIC and secondary somatosensory cortex following tracheal inoculation, whereas lung inoculations of virus resulted in more infected cells in the caudal insular regions (Table 2). There was no evidence of any unilaterality with respect to the infection patterns in the subcortical or cortical nuclei identified following tracheal inoculation with virus, whereas virally infected cells were typically confined to the contralateral primary and secondary somatosensory regions, following lung inoculations (suggesting limited or no labeling of cortico-cortical projections at this time point).

Dual HSV-1 H129 mapping of tracheal and lung sensory pathways

We performed a series of experiments in which animals were simultaneously inoculated with HSV-1 H129 tdTomato into the trachea and HSV-1 H129 EGFP into the lung to assess the degree of convergence of upper and lower airway afferent pathways onto common populations of neurons in the brain. In these animals, the overall central organization of the pathways arising from the trachea and lungs was comparable to that identified with single viral tracing as described above. Evidence for co-infected cells in the brainstem was confined to a minimal number of cells in the nucleus of the solitary tract and paratrigeminal nucleus at early-infection time points, suggesting that convergence of afferent inputs in the lower brainstem may be uncommon. Indeed, relatively few regions of the brain in receipt of afferent input from both the trachea and lungs showed evidence for dually infected cells, with the exception of the preautonomic cell groups in the pontine locus coeruleus and the paraventricular nucleus in the hypothalamus at mid-infection time points which consistently displayed robust dual infections (Fig. 5).

Discussion

Complex sensations arise from the airways and lungs in health and disease, indicating that stimuli in the respiratory system are transmitted to cortical brain regions where perception and cognition are encoded (Davenport and Vovk 2009). However, little is known about the regions of

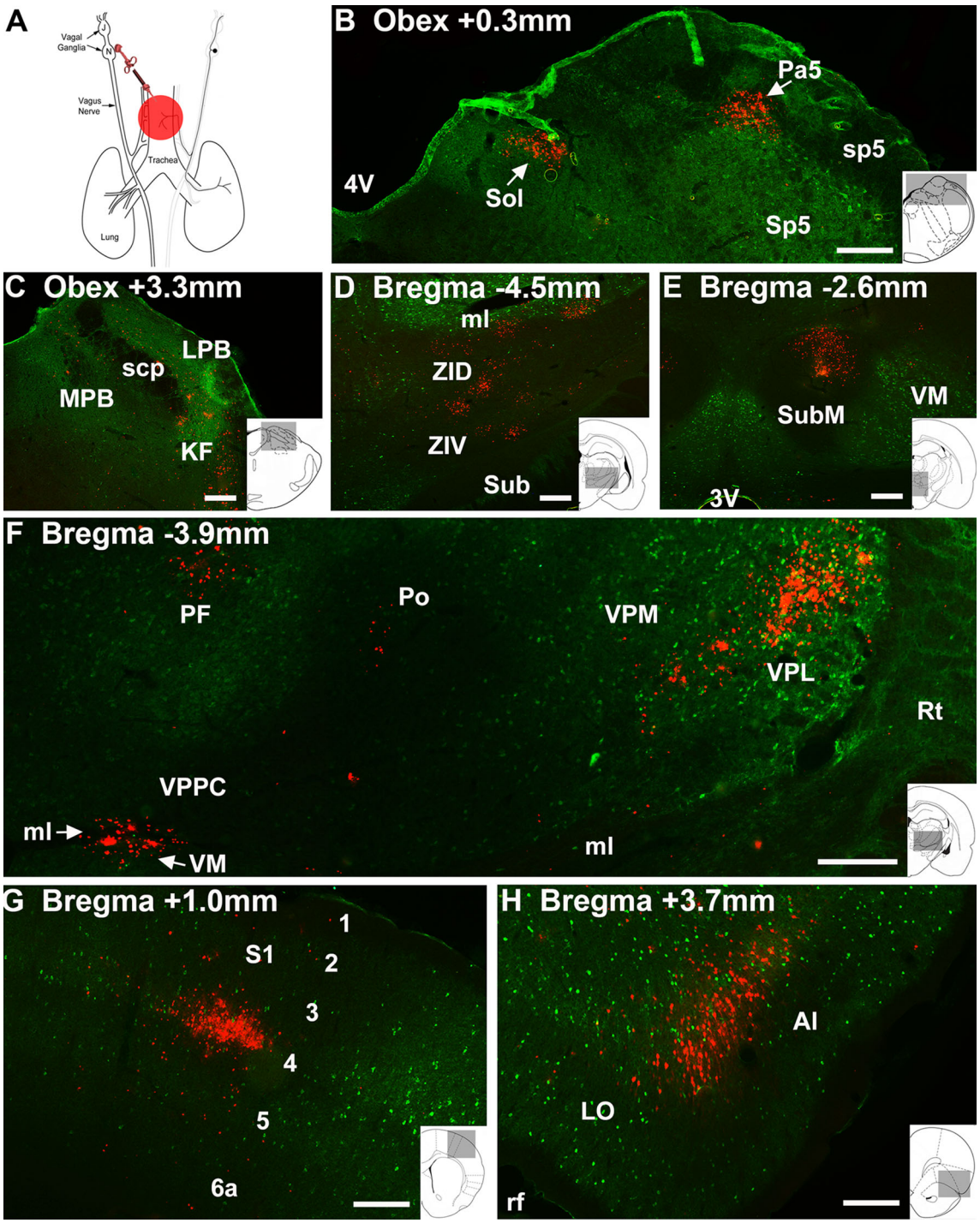

Fig. 3 Representative photomicrographs showing anterograde circuit tracing from the extrathoracic trachea with HSV-1 H129 tdTomato. **a** Schematic representation of the tracheal injection site, showing the vagal nerves and associated nodose (N) and jugular (J) ganglia via which viral transmission to the CNS is mediated. At early time points, tdTomato-expressing (virally infected) cells are first seen in (**b**) sensory relay nuclei in the caudal medulla. At mid time points, viral infection has progressed to the (**c**) pontine, (**d**) subthalamic and (**e**, **f**) thalamic regions. By late time points viral infection is present in (**g**) layer 4 of the somatosensory cortex and (**h**) rostral agranular insular/lateral orbital cortex (RAIC). Sections were counterstained for parvalbumin or calbindin expression (*green*) to provide structural detail. Refer to Table 2 for abbreviations. *Scale bar* represents 200 μm

the brain that are involved in such processes, and even less is known about the brain sensory circuits that interconnect the respiratory system to the higher brain. Furthermore, it is unclear if inputs from the upper airways and lower airways are confined to a single sensory pathway or if there is more than one route for afferent information to reach higher

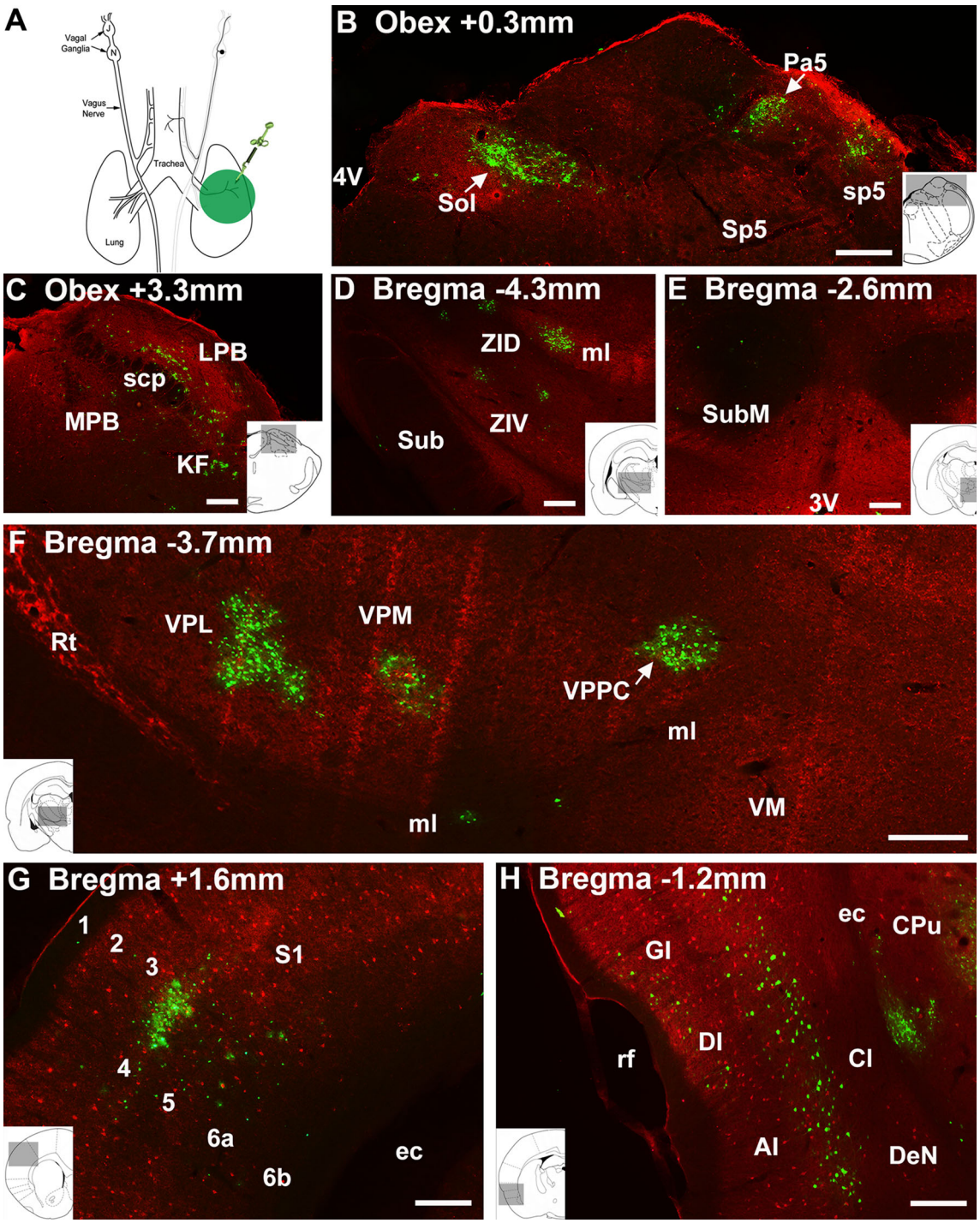

Fig. 4 Representative photomicrographs showing anterograde circuit tracing from the left lung with HSV-1 H129 EGFP. **a** Schematic representation of the lung injection site, showing the vagal nerves and associated nodose (N) and jugular (J) ganglia via which viral transmission to the CNS is mediated. At early time points, EGFP-expressing (virally infected) cells are first seen in (**b**) sensory relay nuclei in the caudal medulla. At mid time points, viral infection has progressed to the (**c**) pontine, (**d**) subthalamic and (**e**, **f**) thalamic regions, although note the near absence of infection in the zona incerta (ventral and dorsal) and submedius and the appearance of infection in the ventral posterior parvicellular thalamus compared to that following tracheal inoculation (compare Fig. 3). By late time points, viral infection is present in the granular and dysgranular insular (**g**) and layer 4 of the somatosensory cortex (**h**). Sections were counterstained for parvalbumin or calbindin expression (*red*) to provide structural detail. Refer to Table 2 for abbreviations. *Scale bar* represents 200 μm

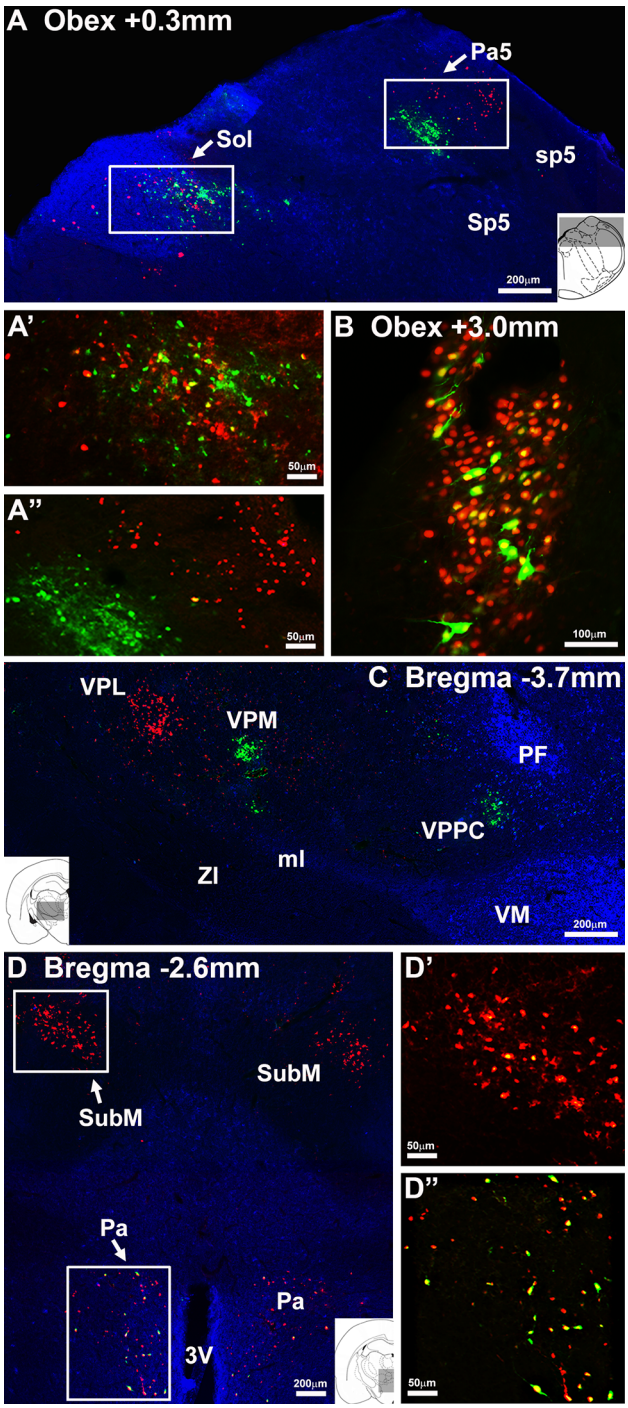

◀**Fig. 5** Representative photomicrographs showing dual simultaneous anterograde circuit tracing from both the trachea and left lung with HSV-1 H129 tdTomato and HSV-1 H129 EGFP, respectively. In the caudal medulla (**a**) populations of tdTomato or EGFP expressing (virally infected) cells are first seen in (**a′**) the nucleus of the solitary tract and (**a″**) the paratrigeminal nucleus. In these sensory relay nuclei, relatively few cells show evidence of dual infection (*yellow* cells). By contrast in (**b**) the pontine locus coeruleus, many dual infected cells were routinely observed. Within the diencephalic regions, largely distinct populations of cells were anterogradely labeled in (**c**) the ventrobasal thalamus. Note the absence of tdTomato expression (tracheal pathway, **c**) in the ventral posterior parvicellular thalamus and EGFP expression (lung pathway, **d** and **d′**) in the submedius nucleus. In the hypothalamus, dual labeled neurons in the paraventricular nucleus (**d″**) were routinely observed. None of the animals tested had successful dual tracing to cortical regions. Sections were counterstained for parvalbumin or calbindin expression (*blue*) to provide structural detail. Refer to Table 2 for abbreviations

levels of the neuraxis. The results from the present study recapitulate our previous studies mapping the ascending sensory pathways arising from the upper airways, showing that the extrathoracic airways project sensory pathways via brainstem and thalamic relays to cortical brain regions which notably include the primary and secondary sensory cortices and the RAIC (McGovern et al. 2012a, b). Indeed, much of this circuitry resembles that known to be important for noxious somatosensation (Jasmin et al. 2004; Tang et al. 2009; Whitt et al. 2013). Furthermore, we show that the primary sensory innervation to the respiratory system is not homogeneous, but rather differs with respect to the likely ganglionic origin and phenotype of their sensory neuron terminals. This coincides with differences in the central organization of the ascending sensory circuits arising from the trachea versus the lungs, the latter displaying projections to distinct thalamic and cortical nuclei thought to be involved in processing visceral sensations. These data provide novel insights into where in the brain respiratory sensations are encoded and may suggest reasons why airway sensations differ qualitatively at different levels of the respiratory tree.

Evidence for multiple central neural pathways mediating respiratory sensations

Functional brain imaging in humans during experimentally induced dyspnea or irritant inhalation evoked urge to cough shows neural activity in the brain encompassing a widely distributed network thought to be integral for processing of sensations arising from the airways (Davenport et al. 1986; Corfield et al. 1995; Mazzone et al. 2007; McKay et al. 2008; Pattinson et al. 2009; Farrell et al. 2012; Raux et al. 2013). For example, inhalation of the nociceptive C-fiber stimulant capsaicin, to evoke laryngeal irritation, induces neural activity in the anterior insular and somatosensory cortex of healthy humans that is thought to encode aspects of sensory discrimination relating to stimulus intensity and perception (Mazzone et al. 2007; Farrell et al. 2012). Activations are also seen in motor cortical regions that enable behavioral control of coughing and in orbital and cingulate cortices, regions that may be involved in the affective or emotive aspects of airways irritation. Studies of experimentally induced dyspnea (evoked by CO_2 inhalation or breath-holding) similarly report neural activations

in somatosensory, motor and limbic brain regions, indicating that some homogeneity may exist between the central processes involved in encoding different airway sensations (Corfield et al. 1995; McKay et al. 2008; Pattinson et al. 2009; Raux et al. 2013). However, such studies do not provide insight into cellular organization of regional responses or the connectivity of airway sensory circuits in the brain, nor do they afford the capacity to localize the stimulus to discrete regions of the respiratory tree.

The herpes virus neuroanatomical tracing methods employed in the present study allowed us to localize, at the cellular level, the central termination patterns of sensory pathways arising from different discrete regions of the respiratory tree. Furthermore, by monitoring the time-dependent nature of the viral infection in the CNS, we can provide insight into the possible interconnectivity of the brain regions in receipt of airway sensory neural input. We have previously validated this viral tracing method (McGovern et al. 2012a, b) and employed the wild-type HSV-1 H129 to map the central projections of sensory pathways arising from the extrathoracic trachea (McGovern et al. 2012a). The results from our present study using a fluorescent reporter recombinant of the virus closely resemble the observations made in our original study. Thus, tracheal vagal sensory neurons terminate in both the nucleus of the solitary tract and the paratrigeminal nucleus in the brainstem and connect to cortical regions via at least two ascending circuits, one of which projects via the trigeminothalamocortical tracts to the primary and secondary sensory cortices and the second via a thalamolimbic circuit to the RAIC. Indeed, the organization of these two pathways is remarkably similar to the lateral and medial ascending pain pathways that have been described for somatosensation (Jasmin et al. 2004; Tang et al. 2009; Whitt et al. 2013). Consistent with this, we have previously shown in humans with functional brain imaging that the pattern of neural activation associated with laryngeal irritation and the urge to cough is strikingly similar to that observed following noxious stimuli applied to the skin (Mazzone et al. 2009).

Previous neuroanatomical and functional studies in rodents have shown that viscerosensory (but not somatosensory) pathways have strong projections via brainstem parabrachial nuclei to the parvicellular region of the ventrobasal thalamus and onto the granular or dysgranular insular cortices (Allen et al. 1991; Bester et al. 1999; Cechetto 2013). This pathway is thought to be important for transmitting visceral sensations to the brain, but our present and previous studies are yet to find any evidence for tracheal sensory projections to the brain via this circuit. Interestingly, however, our present data suggest that while sensory neurons innervating the lung and trachea may terminate in overlapping medullary regions (the nucleus of the solitary tract and the paratrigeminal nucleus), their ascending organization is in part distinct, with a substantial number of lung afferents projecting to the higher brain via the putative viscerosensory pathway. Thus, we found (in a time-dependent manner) a more robust HSV-1 H129 infection in the parabrachial nuclei following lung (compared to trachea) inoculation, as well as infections in the parvicellular ventrobasal thalamus and granular/dysgranular insular cortices. Indeed, whereas the trachea had strong projections to the ventral posterolateral thalamus, submedius thalamus, mediodorsal thalamus, reticular thalamus, zona incerta, secondary somatosensory cortices and RAIC, comparable termination patterns arising from the lung were either less numerous or absent (Fig. 6). Nevertheless, we also noted commonalities in the ascending pathways to the ventral posteromedial thalamus and primary somatosensory cortices.

It was interesting to note that although lung inoculation with HSV-1 H129 resulted in significantly fewer vagal sensory neurons infected compared to tracheal inoculations, the total number of neurons subsequently infected in the brainstem was not different between the two. Indeed, our data suggest that (at least in the nucleus of the solitary tract) there may be significantly more divergence of lung versus tracheal primary afferent inputs onto second-order neurons, effectively meaning that more second-order neurons are synaptically connected to each lung primary afferent neuron compared to each tracheal primary afferent neuron. The functional relevance of this divergence is unclear. However, one could speculate that this may contribute to differences in the fidelity of sensory processing arising from the upper versus lower airways.

Our dual tracing studies showed cellular convergence of tracheal and lung circuits in regions such as locus coeruleus and paraventricular nucleus of the hypothalamus, nuclei with well-defined involvement in the control of autonomic functions. However, we noted little evidence for convergence at other brain sites into which tracheal and lung afferent pathways project, including in brainstem regions where primary afferents terminate. This would also suggest the existence of both common and unique pathways to the brain from the upper and lower airways. However, the lack of extensive co-infection in the dual tracing studies should be interpreted with some caution as previous studies with herpes viruses have shown that even when the number of available virions is high, very few (on average less than seven) of the incoming genomes are expressed in an infected cell (Kobiler et al. 2010). Furthermore, the capacity of a cell to replicate different viral recombinants, even if the recombinants are isogenic, is highly dependent on both viruses reaching the cell in close temporal proximity (Banfield et al. 2003), which may not occur uniformly in all brain regions identified in our

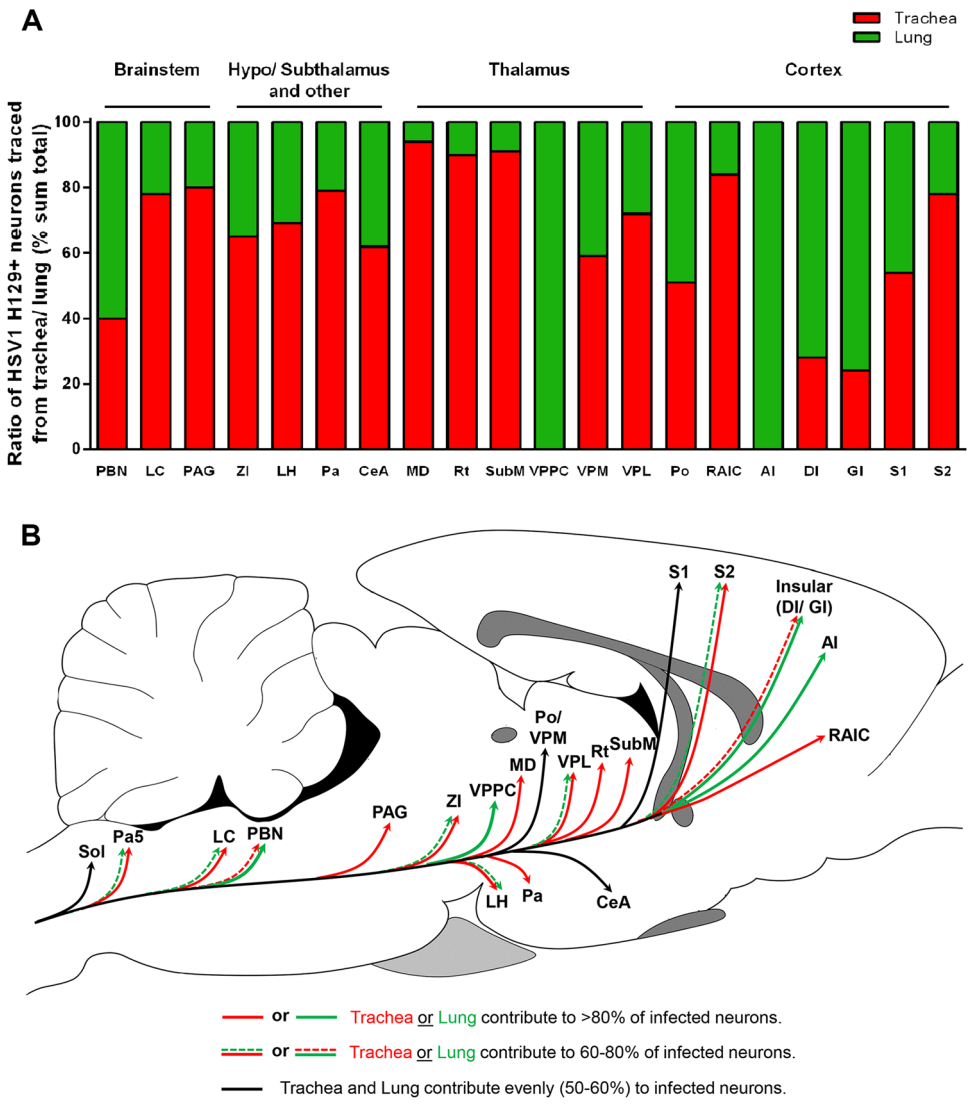

Fig. 6 Organization of ascending sensory circuits arising from the trachea (*red*) versus lung (*green*) as revealed by HSV-1 H129 viral tracing. **a** The ratio of infected neurons in various brainstem and forebrain regions following tracheal or lung inoculation. **b** A sagittal schematic of the rat brain summarizing the proposed circuitry. *Black lines* denote regions to which both tracheal and lung airway sensory pathways equally project. *Red* and *green solid lines* show dominant tracheal and lung projections, respectively. *Dashed lines* indicate disproportionately less innervation. Note, some brain regions omitted for clarity. Refer to Table 2 for abbreviations

tracing studies. These characteristics have significant implications in terms of the efficiency of dual tracing attempts and, therefore while the presence of co-infection in a single neuron can be interpreted with confidence as convergence between two pathways, an absence of co-infection does not negate the possibility that cellular convergence occurs. Nevertheless, when considered in conjunction with the findings from our single viral tracing experiments, the data provide additional evidence for both similarities and differences in the ascending pathways originating from the upper and lower airways.

Although a large body of evidence has detailed the anterograde transneuronal motility of HSV-1 H129, it is important to note that a recent study has called into question the specificity of this virus as an anterograde-only neuronal circuit tracer. In a series of elegant experiments, Wojaczynski and colleagues (2014) showed definitively that HSV-1 H129 maintains some capacity to infect neural circuits via retrograde transynaptic processes, albeit at a significantly delayed temporal rate. This has implications for interpreting tracing outcomes after long survival periods, more so than for experiments with short- to mid-term durations. In our own studies, we have reported HSV-1 H129 infection in sympathetic postganglionic neurons following tracheal injections, consistent with retrograde infection of first-order sympathetic neurons that innervate the airways (McGovern et al. 2012a). However, even after long survival periods (144 h), we do not see infected cells in the intermediolateral cell column (the location of sympathetic preganglionic neurons that would synapse on to infected postganglionic neurons) arguing against significant retrograde transneuronal infection from the airways per se. Similar findings have been reported from the stomach wall using this viral tool (Rinaman and Schwartz 2004). Nevertheless, we cannot rule out that retrograde transneuronal movement could occur at synapses within

the central nervous system. For example, it is conceivable that infected ascending neurons in the nucleus of the solitary tract or paratrigeminal nucleus (or elsewhere) may receive descending inputs from forebrain nuclei which could be retrogradely labeled after longer survival periods. As an argument against this occurring on a widespread scale in our study, much of the circuitry identified is highly consistent with well-described somatic and visceral sensory pathways in the brain.

Somatic and visceral sensory neuronal phenotypes innervate the airways

Pulmonary sensory neurons are not homogeneous, and there exists a variety of ways to classify different sensory subtypes. One such way is to identify the particular vagal ganglion from which they are derived, as the jugular and nodose vagal ganglia are embryologically distinct tissues. Jugular ganglia neurons develop out of the neural crest cell lineage that forms much of the somatic nervous system, whereas nodose neurons are derived from the epibranchial placodes that form the visceral and autonomic nervous systems (Baker and Schlosser 2005). The present study in rats is consistent with previous studies in mice and guinea pigs, in that the sensory innervation of the extrathoracic trachea is predominately derived from the jugular neural crest inasmuch as the neurons express molecular markers (TRKA, PPT-A) characteristic of jugular neurons. By contrast, the lung appears to be in receipt of both neural crest and placodal (nodose) neurons, the latter identified by their expression of TRKB and the purinergic receptor P2X2 (present data; Undem et al. 2004; Kwong et al. 2008; Nassenstein et al. 2010; Lieu et al. 2011). Interestingly, in developing mouse and chick embryos there is evidence for unique transcription factors driving jugular neurons to predominately terminate in the trigeminal nuclei in the brainstem compared to nodose neurons, which are guided into the nucleus of the solitary tract (D'Autréaux et al. 2011). This raises the possibility that sensory neurons originating from jugular and nodose ganglia may differentially input to somatic versus visceral ascending circuits in the brain. Indeed, we noted differences in the pattern of inputs from the trachea and lung to the paratrigeminal nucleus and nucleus of the solitary tract, and this is somewhat consistent with our circuit tracing outcomes showing mostly somatosensory-like projection pathways arising from the trachea compared to a mixed visceral-like and somatosensory-like projection pathway from the lung. However, confirmation of whether different vagal afferent populations input to distinct ascending circuits in the brain awaits the development of more sophisticated methods to map the central neural circuits innervated by single airway sensory neuron subtypes.

Significance

Clinical observations would indicate that airway sensations in humans differ qualitatively at different levels of the respiratory tree and the capacity to localize the site of a stimulus diminishes in more distal airways (Morice et al. 2006). In experimental settings, capsaicin inhalation produces an unpleasant but discretely localized noxious sensation in the laryngotracheal airways that is described as itching or scratching in the larynx (Mazzone et al. 2007), but when administered intravenously (via the superior vena cava) to the pulmonary vascular bed it produces a diffuse 'raw burning' sensation in the chest (Winning et al. 1986). This might indicate that differences exist in the sensory pathways arising from different regions of the respiratory tract, which in turn may have implications in the manifestation of sensory abnormalities in respiratory diseases. Indeed, airway vagal sensory nerve stimulation can give rise to both dyspnea and the urge to cough, two very different sensory experiences (Mazzone et al. 2007; Burki and Lee 2010).

An interesting observation in the present study was the less frequent and less robust nature of the inputs to the zona incerta, submedius thalamus and reticular nucleus of the thalamus arising from the lung compared to the trachea. These subcortical nuclei play an important role in thalamic gating of ascending sensations (zona incerta and reticular thalamus) (Lee et al. 1994; Liu et al. 1995; Trageser and Keller 2004; Trageser et al. 2006) and/or in descending inhibitory control systems (the submedius nucleus of the thalamus) (Zhang et al. 1997; Jasmin et al. 2004; Huo et al. 2008; Tang et al. 2009). Thus, neurons from the zona incerta and reticular thalamus provide GABAergic inhibitory inputs to the sensory thalamic nuclei that can reduce the amount of sensory information relayed to the cortex (Lee et al. 1994; Liu et al. 1995; Wang et al. 2005). Interestingly, it is well accepted that the pain-relieving effects of transcranial magnetic motor cortex stimulation in humans and animals reflects the activation of a motor cortex–zona incerta–thalamus suppressive circuit (Lucas et al. 2011; Cha et al. 2013). Similarly, the submedius thalamus has well-described projections to the RAIC, which in turn can provide descending inhibitory control (via projections to the midbrain periaqueductal gray) to reduce primary sensory inputs to the spinal cord (Zhang et al. 1997; Jasmin et al. 2004; Huo et al. 2008; Tang et al. 2009). Whether similar circuits can regulate vagal afferent inputs from the airways is unknown, although the present data might suggest that the upper airways has a greater propensity for sensory inputs to the brain to be filtered or inhibited, perhaps (albeit speculative) important for the increased likelihood of sensory neuron activation in the proximal airways, due to their intimate relationship with the external

environment. It is interesting to note that attentional distraction inhibits the affective, but not the sensory, dimensions of induced dyspnea (von Leupoldt et al. 2007, 2011), unlike the sensory component of the urge to cough from the upper airways, which is readily modifiable by cognitive manipulations (Leech et al. 2012, 2013).

Concluding remarks

The results of the present study suggest the existence of multiple sensory pathways in the brain arising from the airways and lungs, perhaps differentiated by the dual somatic and visceral nature of the airway sensory innervation. The data highlight the primary afferent terminations into the paratrigeminal nucleus and the nucleus of the solitary tract, raising questions about the functional significance of these two brainstem integration nuclei with respect to the processing airway sensations. Perhaps, this brainstem organization similarly reflects the distinct primary afferent pathways, which in turn differentially contribute to the higher brain circuits described herein. If true, this has important implications for interpreting the nature of sensations arising from different parts of the airways and lungs, and could lead to the identification of novel targets for relieving abnormal respiratory sensations that are common in lung disease.

Acknowledgments This research was supported by grants to Dr Mazzone and Dr Farrell from the National Health and Medical Research Council (NHMRC) of Australia [566734, 454776, 1025589]. The authors would like to thank Professor Lynn Enquist and Dr Halina Staniszewska Goraczniak (Princeton University, Princeton, NJ, USA) for their generosity in supplying the original wild-type H129 strain of HSV-1 and to Professor Stacey Efstathiou (University of Cambridge, UK) for supplying the tdTomato expression cassette.

References

Allen GV, Saper CB, Hurley KM, Cechetto DF (1991) Organization of visceral and limbic connections in the insular cortex of the rat. J Comp Neurol 311(1):1–16

Baker CV, Schlosser G (2005) The evolutionary origin of neural crest and placodes. J Exp Zool B Mol Dev Evol 304:269–273

Banfield BW, Kaufman JD, Randall JA, Pickard GE (2003) Development of pseudorabies virus strains expressing red fluorescent proteins: new tools for multisynaptic labeling applications. J Virol 77(18):10106–10112

Bester H, Bourgeais L, Villanueva L, Besson JM, Bernard JF (1999) Differential projections to the intralaminar and gustatory thalamus from the parabrachial area: a PHA-L study in the rat. J Comp Neurol 405(4):421–449

Burkey AR, Carstens E, Jasmin L (1999) Dopamine reuptake inhibition in the rostral agranular insular cortex produces antinociception. J Neurosci 19(10):4169–4179

Burki NK, Lee LY (2010) Blockade of airway sensory nerves and dyspnea in humans. Pulm Pharmacol Ther 23(4):279–282

Cechetto DF (2013) Cortical control of the autonomic nervous system. Exp Physiol 99(2):326–331

Cha M, Ji Y, Masri R (2013) Motor cortex stimulation activates the incertothalamic pathway in an animal model of spinal cord injury. J Pain 14(3):260–269

Corfield DR, Fink GR, Ramsay SC, Murphy K, Harty HR, Watson JD, Adams L, Frackowiak RS, Guz A (1995) Evidence for limbic system activation during CO2-stimulated breathing in man. J Physiol 488(Pt 1):77–84

D'Autréaux F, Coppola E, Hirsch MR, Birchmeier C, Brunet JF (2011) Homeoprotein Phox2b commands a somatic-to-visceral switch in cranial sensory pathways. Proc Natl Acad Sci USA 108(50):20018–20023

Davenport PW, Vovk A (2009) Cortical and subcortical central neural pathways in respiratory sensations. Respir Physiol Neurobiol 1:72–86

Davenport PW, Friedman WA, Thompson FJ, Franzén O (1986) Respiratory-related cortical potentials evoked by inspiratory occlusion in humans. J Appl Physiol 60(6):1843–1848

Evans KC (2010) Cortico-limbic circuitry and the airways: insights from functional neuroimaging of respiratory afferents and efferents. Biol Psychol 84(1):13–25 (Review)

Farrell MJ, Cole LJ, Chiapoco D, Egan GF, Mazzone SB (2012) Neural correlates coding stimulus level and perception of capsaicin-evoked urge-to-cough in humans. Neuroimage 61(4):1324–1335

Garner JA, LaVail JH (1999) Differential anterograde transport of HSV type 1 viral strains in the murine optic pathway. J Neurovirol 5(2):140–150

Haxhiu MA, Kc P, Moore CT, Acquah SS, Wilson CG, Zaidi SI, Massari VJ, Ferguson DG (2005) Brain stem excitatory and inhibitory signaling pathways regulating bronchoconstrictive responses. J Appl Physiol. 98(6):1961–1982 (Review)

Huo FQ, Qu CL, Li YQ, Tang JS, Jia H (2008) GABAergic modulation is involved in the ventrolateral orbital cortex 5-HT 1A receptor activation-induced antinociception in the rat. Pain 139(2):398–405

Jasmin L, Rabkin SD, Granato A, Boudah A, Ohara PT (2003) Analgesia and hyperalgesia from GABA-mediated modulation of the cerebral cortex. Nature 424(6946):316–320

Jasmin L, Burkey AR, Granato A, Ohara PT (2004) Rostral agranular insular cortex and pain areas of the central nervous system: a tract-tracing study in the rat. J Comp Neurol 468(3):425–440

Kalous A, Keast JR (2010) Conditioning lesions enhance growth state only in sensory neurons lacking calcitonin gene-related peptide and isolectin B4-binding. Neuroscience 166(1):107–121

Kobiler O, Lipman Y, Therkelsen K, Daubechies I, Enquist LW (2010) Herpesviruses carrying a Brainbow cassette reveal replication and expression of limited numbers of incoming genomes. Nat Commun 1:146

Kummer W, Fischer A, Kurkowski R, Heym C (1992) The sensory and sympathetic innervation of guinea-pig lung and trachea as studied by retrograde neuronal tracing and double-labelling immunohistochemistry. Neuroscience 49(3):715–737

Kwong K, Kollarik M, Nassenstein C, Ru F, Undem BJ (2008) P2X2 receptors differentiate placodal vs. neural crest C-fiber phenotypes innervating guinea pig lungs and esophagus. Am J Physiol Lung Cell Mol Physiol 295(5):L858–L865

Larson SD, Schelegle ES, Hyde DM, Plopper CG (2003) The three-dimensional distribution of nerves along the entire intrapulmonary airway tree of the adult rat and the anatomical relationship between nerves and neuroepithelial bodies. Am J Respir Cell Mol Biol 28(5):592–599

Lee SM, Friedberg MH, Ebner FF (1994) The role of GABA-mediated inhibition in the rat ventral posterior medial thalamus. I. Assessment of receptive field changes following thalamic reticular nucleus lesions. J Neurophysiol 71:1702–1715

Leech J, Mazzone SB, Farrell MJ (2012) The effect of placebo conditioning on capsaicin-evoked urge to cough. Chest 142(4):951–957

Leech J, Mazzone SB, Farrell MJ (2013) Brain activity associated with placebo suppression of the urge-to-cough in humans. Am J Respir Crit Care Med 188(9):1069–1075

Lieu T, Kollarik M, Myers AC, Undem BJ (2011) Neurotrophin and GDNF family ligand receptor expression in vagal sensory nerve subtypes innervating the adult guinea pig respiratory tract. Am J Physiol Lung Cell Mol Physiol 300(5):L790–L798

Liu XB, Warren RA, Jones EG (1995) Synaptic distribution of afferents from reticular nucleus in ventroposterior nucleus of cat thalamus. J Comp Neurol. 352:187–202

Lo L, Anderson DJ (2011) A Cre-dependent, anterograde transsynaptic viral tracer for mapping output pathways of genetically marked neurons. Neuron 72(6):938–950

Lucas JM, Ji Y, Masri R (2011) Motor cortex stimulation reduces hyperalgesia in an animal model of central pain. Pain 152(6):1398–1407

Mazzone SB, Canning BJ (2013) Autonomic neural control of the airways. Handb Clin Neurol. 117:215–228

Mazzone SB, McGovern AE (2006) Na^+–K^+–$2Cl^-$ cotransporters and Cl^- channels regulate citric acid cough in guinea pigs. J Appl Physiol 101(2):635–643

Mazzone SB, McGovern AE (2008) Immunohistochemical characterization of nodose cough receptor neurons projecting to the trachea of guinea pigs. Cough 4:9

Mazzone SB, Mori N, Canning BJ (2005) Synergistic interactions between airway afferent nerve subtypes regulating the cough reflex in guinea-pigs. J Physiol 569(Pt 2):559–573

Mazzone SB, McLennan L, McGovern AE, Egan GF, Farrell MJ (2007) Representation of capsaicin-evoked urge-to-cough in the human brain using functional magnetic resonance imaging. Am J Respir Crit Care Med 176(4):327–332

Mazzone SB, McGovern AE, Koo K, Farrell MJ (2009) Mapping supramedullary pathways involved in cough using functional brain imaging: comparison with pain. Pulm Pharmacol Ther 22(2):90–96

Mazzone SB, Cole LJ, Ando A, Egan GF, Farrell MJ (2011) Investigation of the neural control of cough and cough suppression in humans using functional brain imaging. J Neurosci 31(8):2948–2958

McGovern AE, Mazzone SB (2010) Characterization of the vagal motor neurons projecting to the Guinea pig airways and esophagus. Front Neurol 1:153

McGovern AE, Davis-Poynter N, Farrell MJ, Mazzone SB (2012a) Transneuronal tracing of airways-related sensory circuitry using Herpes Simplex Virus 1, strain H129. Neuroscience 207:148–166

McGovern AE, Davis-Poynter N, Rakoczy J, Phipps S, Simmons DG, Mazzone SB (2012b) Anterograde neuronal circuit tracing using a genetically modified herpes simplex virus expressing EGFP. J Neurosci Methods 209(1):158–167

McKay LC, Adams L, Frackowiak RS, Corfield DR (2008) A bilateral cortico-bulbar network associated with breath holding in humans, determined by functional magnetic resonance imaging. Neuroimage 40(4):1824–1832

Morice AH, McGarvey L, Pavord I et al (2006) Recommendations for the management of cough in adults. Thorax 61(Suppl 1):1–24

Nassenstein C, Taylor-Clark TE, Myers AC, Ru F, Nandigama R, Bettner W, Undem BJ (2010) Phenotypic distinctions between neural crest and placodal derived vagal C-fibres in mouse lungs. J Physiol 588(Pt 23):4769–4783

Pattinson KT, Governo RJ, MacIntosh BJ, Russell EC, Corfield DR, Tracey I, Wise RG (2009) Opioids depress cortical centers responsible for the volitional control of respiration. J Neurosci 29(25):8177–8186

Paxinos G, Carrive P, Wang H, Wang P-Y (1999a) Chemoarchitectonic atlas of the rat brainstem. Academic Press, San Diego

Paxinos G, Kus L, Ashwell KWS, Watson C (1999b) Chemoarchitectonic atlas of the rat forebrain. Academic Press, San Diego

Raux M, Tyvaert L, Ferreira M, Kindler F, Bardinet E, Karachi C, Morelot-Panzini C, Gotman J, Pike GB, Koski L, Similowski T (2013) Functional magnetic resonance imaging suggests automatization of the cortical response to inspiratory threshold loading in humans. Respir Physiol Neurobiol 189(3):571–580

Riccio MM, Kummer W, Biglari B, Myers AC, Undem BJ (1996) Interganglionic segregation of distinct vagal afferent fibre phenotypes in guinea-pig airways. J Physiol 496(Pt 2):521–530

Rinaman L, Schwartz G (2004) Anterograde transneuronal viral tracing of central viscerosensory pathways in rats. J Neurosci 24(11):2782–2786

Shannon R, Baekey DM, Morris KF, Nuding SC, Segers LS, Lindsey BG (2004) Production of reflex cough by brainstem respiratory networks. Pulm Pharmacol Ther 17(6):369–376

Song CK, Schwartz GJ, Bartness TJ (2008) Anterograde transneuronal viral tract tracing reveals central sensory circuits from white adipose tissue. Am J Physiol Regul Integr Comp Physiol 296(3):R501–R511

Tang JS, Qu CL, Huo FQ (2009) The thalamic nucleus submedius and ventrolateral orbital cortex are involved in nociceptive modulation: a novel pain modulation pathway. Prog Neurobiol 89(4):383–389

Trageser JC, Keller A (2004) Reducing the uncertainty: gating of peripheral inputs by zona incerta. J Neurosci 24(40):8911–8915

Trageser JC, Burke KA, Masri R, Li Y, Sellers L, Keller A (2006) State-dependent gating of sensory inputs by zona incerta. J Neurophysiol 96(3):1456–1463

Undem BJ, Chuaychoo B, Lee MG, Weinreich D, Myers AC, Kollarik M (2004) Subtypes of vagal afferent C-fibres in guinea-pig lungs. J Physiol 556(3):905–917

Vaughan CH, Bartness TJ (2012) Anterograde transneuronal viral tract tracing reveals central sensory circuits from brown fat and sensory denervation alters its thermogenic responses. Am J Physiol Regul Integr Comp Physiol 302(9):R1049–R1058

von Leupoldt A, Seemann N, Gugleva T, Dahme B (2007) Attentional distraction reduces the affective but not the sensory dimension of perceived dyspnea. Respir Med 101(4):839–844

von Leupoldt A, Chan PY, Bradley MM, Lang PJ, Davenport PW (2011) The impact of anxiety on the neural processing of respiratory sensations. Neuroimage 55(1):247–252

Wang J, Huo FQ, Li YQ, Chen T, Han F, Tang JS (2005) Thalamic nucleus submedius receives GABAergic projection from thalamic reticular nucleus in the rat. Neuroscience 134(2):515–523

Whitt JL, Masri R, Pulimood NS, Keller A (2013) Pathological activity in mediodorsal thalamus of rats with spinal cord injury pain. J Neurosci 33(9):3915–3926

Winning AJ, Hamilton RD, Shea SA, Guz A (1986) Respiratory and cardiovascular effects of central and peripheral intravenous injections of capsaicinin man: evidence for pulmonary chemosensitivity. Clin Sci (Lond) 71(5):519–526

Wojaczynski GJ, Engel EA, Steren KE, Enquist LW, Patrick Card J (2014) The neuroinvasive profiles of H129 (herpes simplex virus type 1) recombinants with putative anterograde-only transneuronal spread properties. Brain Struc Funct

Zhang S, Tang JS, Yuan B, Jia H (1997) Involvement of the frontal ventrolateral orbital cortex in descending inhibition of nociception mediated by the periaqueductal gray in rats. Neurosci Lett 224(2):142–146